

## Wave Breaking Induced by Opposing Currents in Submerged Vegetation Canopies

Hu, Z.; Lian, S.; Zitman, T.; Wang, H.; He, Z.; Wei, H.; Ren, L.; Uijtewaal, W.; Suzuki, T.

**DOI**

[10.1029/2021WR031121](https://doi.org/10.1029/2021WR031121)

**Publication date**

2022

**Document Version**

Final published version

**Published in**

Water Resources Research

**Citation (APA)**

Hu, Z., Lian, S., Zitman, T., Wang, H., He, Z., Wei, H., Ren, L., Uijtewaal, W., & Suzuki, T. (2022). Wave Breaking Induced by Opposing Currents in Submerged Vegetation Canopies. *Water Resources Research*, 58(4), Article e2021WR031121. <https://doi.org/10.1029/2021WR031121>

**Important note**

To cite this publication, please use the final published version (if applicable). Please check the document version above.

**Copyright**

Other than for strictly personal use, it is not permitted to download, forward or distribute the text or part of it, without the consent of the author(s) and/or copyright holder(s), unless the work is under an open content license such as Creative Commons.

**Takedown policy**






Please contact us and provide details if you believe this document breaches copyrights. We will remove access to the work immediately and investigate your claim.

# Water Resources Research®

## RESEARCH ARTICLE

10.1029/2021WR031121

## Wave Breaking Induced by Opposing Currents in Submerged Vegetation Canopies

Z. Hu<sup>1,2,3</sup> , S. Lian<sup>4</sup>, T. Zitman<sup>5</sup>, H. Wang<sup>1</sup>, Z. He<sup>1,3</sup> , H. Wei<sup>1,6</sup>, L. Ren<sup>7</sup> , W. Uijttewaai<sup>5</sup> , and T. Suzuki<sup>5,8</sup> 

### Key Points:

- A generic  $C_D$ - $Re$  relation for various current-wave combinations has been proposed
- Opposing currents can trigger wave breaking in submerged canopies, leading to greater wave dissipation than following currents
- An analytical model is developed to assess the contribution of wave breaking as indirect wave dissipation by vegetation

<sup>1</sup>School of Marine Sciences, Sun Yat-Sen University, and Southern Marine Science and Engineering Guangdong Laboratory (Zhuhai), Zhuhai, China, <sup>2</sup>Guangdong Provincial Key Laboratory of Marine Resources and Coastal Engineering, Guangzhou, China, <sup>3</sup>Pearl River Estuary Marine Ecosystem Research Station, Ministry of Education, Zhuhai, China, <sup>4</sup>South China Sea Environment Monitoring Center, State Oceanic Administration, Guangzhou, China, <sup>5</sup>Faculty of Civil Engineering and Geosciences, Delft University of Technology, Delft, The Netherlands, <sup>6</sup>Department of Ocean Science, Hong Kong University of Science and Technology, Hong Kong, China, <sup>7</sup>School of Marine engineering and technology, Sun Yat-Sen University, Zhuhai, China, <sup>8</sup>Flanders Hydraulics Research, Antwerp, Belgium

### Supporting Information:

Supporting Information may be found in the online version of this article.

### Correspondence to:

L. Ren,  
[renlei7@mail.sysu.edu.cn](mailto:renlei7@mail.sysu.edu.cn)

### Citation:

Hu, Z., Lian, S., Zitman, T., Wang, H., He, Z., Wei, H., et al. (2022). Wave breaking induced by opposing currents in submerged vegetation canopies. *Water Resources Research*, 58, e2021WR031121. <https://doi.org/10.1029/2021WR031121>

Received 27 AUG 2021

Accepted 14 MAR 2022

**Abstract** Wave height attenuation in vegetation canopies is often all attributed to the drag force exerted by vegetation, whereas other potential dissipation process is often neglected. Previous studies without vegetation have found that opposing currents can induce wave breaking and greatly increase dissipation. It is not clear if similar process may also occur in vegetation canopies. We conducted systematic flume experiments to show that wave breaking in opposing currents can occur in vegetated flows, but only in submerged canopies with shear currents above vegetation top. Subsequently, we developed a new analytical model to understand and assess the contribution of both drag-induced dissipation in the lower vegetation layer and current-induced breaking in the upper free layer. A new generic drag coefficient relation was applied in the model to quantify drag-induced dissipation with various current-wave combinations. It shows that breaking induced by opposing currents constitutes an essential part (up to 87%) of the total dissipation, which leads to considerably higher dissipation than the cases with following currents. Breaking can occur with various submergence ratios and with small opposing currents in the submerged vegetation field. It indicates that similar breaking process is likely to occur in real vegetation fields. The present study reveals and quantifies the current-induced wave breaking process that has not been reported before, which can improve our understanding of vegetation wave dissipation capacity in field conditions.

**Plain Language Summary** Nature-based coastal protection has drawn much attention from coastal scientists, engineers, and managers. This measure conserves and (re)creates vegetated coastal wetlands, for example, saltmarshes, mangroves, and seagrasses as buffers to attenuate incident waves and reduce wave load on dikes. The mechanisms of wave dissipation in coastal wetlands have been extensively investigated. Existing studies generally attribute all the dissipation to the drag force exerted by vegetation, whereas indirect wave dissipation that may occur with accompanying tidal currents is generally neglected. By extensive flume experiments, we found that substantial indirect wave dissipation can be induced by triggered breaking. Such process takes place in submerged canopies with a suitable submergence ratio (e.g.,  $1 < \text{water depth/canopy height} < 4.5$ ), where the currents above the submerged canopies is accelerated by the underneath vegetation drag. These insights highlight the importance of previously overlooked indirect wave dissipation in vegetation fields (not by vegetation drag but by breaking), which are likely to occur in shallowly submerged mangrove and saltmarsh canopies. Thus, the knowledge and the model developed in the present study provide a base for more precise predictions of coastal wetlands' protection values.

## 1. Introduction

Coastal wetlands such as mangroves and saltmarshes are increasingly recognized as effective buffers to attenuate incident waves and reduce the load on coastal structures (Leonardi et al., 2018; Ondiviela et al., 2014; Vuik et al., 2018). Because of the valuable coastal defenses service, integrating these vegetated wetlands in nature-based coastal defenses has been proposed (Currin, 2019; Temmerman et al., 2013; van Loon-Steensma et al., 2014, 2016). To bring nature-based coastal defenses into practice, in-depth understanding and quantitative insights of wave dissipation by vegetation (hereafter referred to as WDV) are essential (Bouma et al., 2014).

WDV has been investigated in many previous studies using lab experiments (Lara et al., 2016; Mancheno et al., 2021; Möller et al., 2014; Paul & Gillis, 2015; Yao et al., 2018), field observations (Horstman et al., 2014; Vuik et al., 2016) and theoretical/numerical models (Cao et al., 2015; Chen & Zou, 2019; Dalrymple et al., 1984; Méndez & Losada, 2004; Suzuki et al., 2019).

Located in intertidal areas, mangroves and saltmarsh canopies are commonly subjected to combined current-wave flows (Losada et al., 2016; Ysebaert et al., 2011). Specifically, incident waves propagate into vegetated wetlands in the same direction as the tidal currents during flooding tide. Reversely, waves propagate in the opposite direction as the tidal currents during ebb tide (Garzon et al., 2019). Using the waves as a reference, we designate currents that flow in the same direction as wave propagation (e.g., flooding currents) as following currents, and currents that flow in the opposite direction as wave propagation (e.g., ebb currents) as opposing currents. Previous studies involving the following currents have shown that WDV varies with the ratio of the depth-averaged imposed current velocity and the amplitude of wave orbital velocity ( $\alpha = U_c/U_w$ ; Z. Hu et al., 2014; Li & Yan, 2007; Paul et al., 2012). WDV is suppressed when  $\alpha$  is smaller than one but enhanced when  $\alpha$  is higher. The comparison between following and opposing currents has also been addressed in Maza et al. (2015) and Garzon et al. (2019).

Notably, most studies devote all the WDV to work done by vegetation drag force, whereas other possible wave dissipation mechanism is neglected. Previous studies without vegetation have found that opposing currents can induce partial wave breaking when the ratio between current velocity ( $U$ ) and wave celerity ( $c$ ) reaches certain thresholds (Brevik & Bjørn, 1979; Chen & Zou, 2018; Unna, 1942; Yu, 1952; Zheng et al., 2008). However, it is not clear if similar breaking process exists in vegetated fields with coexisting currents. This unidentified part of WDV can be referred as indirect wave dissipation by vegetation since it is not directly linked to the work done by vegetation drag force. Further investigation of the indirect WDV can potentially complement the existing knowledge on direct WDV, leading to more accurate predictions of the wave attenuation capacity of coastal vegetation fields.

To assess the relative contribution of indirect WDV, accurate quantification of the direct WDV is needed. As a critical parameter determining drag force and direct WDV, vegetation drag coefficient  $C_D$  in following and opposing currents has been obtained by calibrating WDV models against observed wave reduction (H. Chen et al., 2018; Losada et al., 2016). The accuracy of this method depends on the reliability of the predetermined models, and the applicability of the derived  $C_D$  can be limited to specific experiments (Henry et al., 2015). A more direct method is using synchronized velocity ( $u$ ) and force ( $F$ ) measurement and derives  $C_D$  directly from the original Morison equation (Morison et al., 1950). This method can eliminate potential errors from the WDV models. Another advantage of the direct method is that the measured velocity is the velocity in the constriction between adjacent canopy elements, which is an appropriate velocity scale to be used in the relations between  $C_D$  and Reynolds number ( $Re$ ; Etminan et al., 2019; Van Rooijen et al., 2018).

This direct method has been applied in pure waves and waves with following currents cases (H. Chen et al., 2018; Z. Hu et al., 2014; Infantes et al., 2011; van Hespden et al., 2021), and the derived empirical relation of  $C_D$  and  $Re$  (Reynolds number) has been proven to be useful in numerous experiment and numerical studies (Henry et al., 2015; J. Hu et al., 2019; P. L.-F Liu et al., 2015; van Veelen et al., 2021; Wang et al., 2015). However,  $C_D$  in opposing currents is yet to be investigated using this direct method. Applying this method to both following and opposing currents can generate a general empirical relation for various current-wave conditions.

In the present study, we conducted a flume experiment (Figure 1) to mimic wave propagation with accompany currents in stiff vegetation canopies, such as mangroves (Figure S5 in Supporting Information S1). Our main aim is to reveal the mechanism and the relative importance of indirect WDV induced by wave breaking. We included tests with both following and opposing currents ( $\alpha$  varies from  $-2$  to  $4$ ) to reveal the relative importance of wave breaking. Tests with both emergent and submerged conditions are included to show the necessity of a free flow layer for wave breaking. Additionally, various scenarios, including wave height and period, high and low stem densities as well as regularly and randomly arranged canopies were tested (Figure S1 in Supporting Information S1). The obtained data of wave height, velocity and force on the vegetation stems are included in an open data repository (Z. Hu et al., 2020) to facilitate data reuse. A new analytical model is developed to explain the observed WDV with both direct and indirect contributions. The novelty of this model is the quantification of the onset and magnitude of current-induced wave breaking in vegetation canopies. The obtained results are

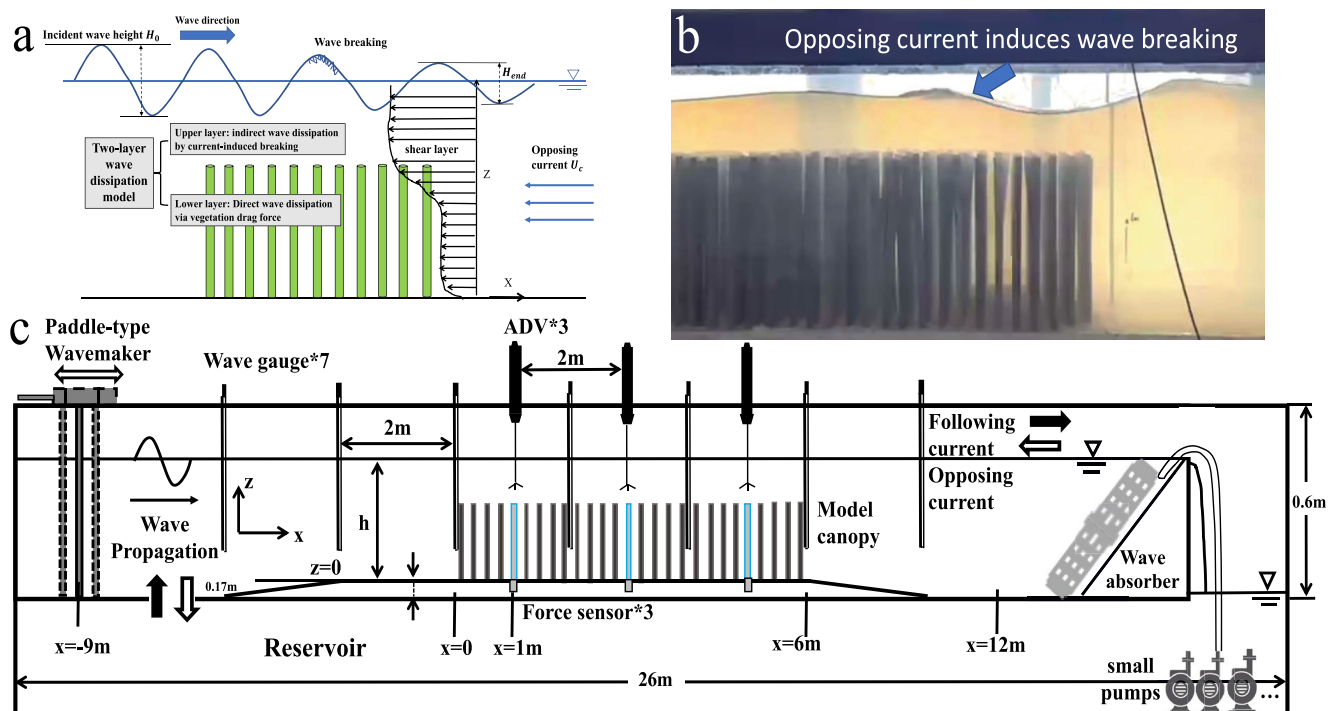


**Figure 1.** (a) A schematic diagram of direct and indirect wave dissipation (wave breaking) in a submerged canopy, (b) a photo of wave breaking induced by opposing currents. A movie of partial wave breaking in the vegetation field can be found at <https://doi.org/10.6084/m9.figshare.13026530>, (c) the flume experiment setup, seven capacitance-type wave gauges were installed along the flume to measure wave height variations. Three pairs of Acoustic Doppler Velocimeters (ADV) and force sensors were deployed to measure in-phase velocity-force on mimic plants for direct  $C_D$  derivation (H. Chen et al., 2018; Yao et al., 2018). Following currents were generated by a circulation pump, whereas opposing currents were generated by a number of small pumps behind the wave absorber.

discussed for their implications in nature-based coastal protections using mangrove forests (Figure S5 in Supporting Information S1).

## 2. Experiments and Analytical Model

### 2.1. Experiment Setup

Experiments were performed in a 26-m-long, 0.6-m-wide, 0.6-m-high wave-current flume in the Hydrodynamics Lab of Sun Yat-sen University (Figure 1c). The mimic canopies were built with stiff wooden rods in the middle of the wave flume (Figure 1c). The canopies were 6-m long and 0.6-m wide, and the height ( $h_v$ ) and diameter ( $b_v$ ) of the rods were 0.25 and 0.01 m, respectively. The length of the canopies was chosen so that it is 3–4 times of the wave length, that is, the canopies can accommodate 3–4 waves in all the tests. They are placed on a plywood false bottom, beneath which three force sensors (M140 by UTILCELL) were placed to measure the acting force on the rods (Figure 1c). Two mimic stem densities ( $N_v = 139$  and  $556$  stems/m<sup>2</sup>), as well as control tests ( $N_v = 0$ ) were tested and referred to as “VD2,” “VD3,” and “VD0,” respectively. These stem densities and stem diameter were identical to those in Z. Hu et al. (2014) to facilitate comparison. Emergent and submerged canopies were achieved by adjusting still water levels in the flume ( $h = 0.20$  and  $0.33$  m). Due to the depth limitation of the flume, the tested submergence ratio of the submerged case is relatively low, that is,  $h/h_v = 1.32$ , which may be considered near-emergent condition (Augustin et al., 2009). Still, following the general definition in Nepf (2012), such condition is defined as submerged condition nonetheless.

Following currents were generated by a circulation pump located close to the wave maker, whereas opposing currents were generated by a set of small pumps located behind the wave absorber (Figure 1). In cases of following currents, the intended water depth and velocity in the vegetation field were controlled by changing the inputs of the pump and the outflow gate at the end of the flume. In cases of opposing currents, we change the number of working pumps to control the water depth and velocity. The fence structure of the wave absorber can help in

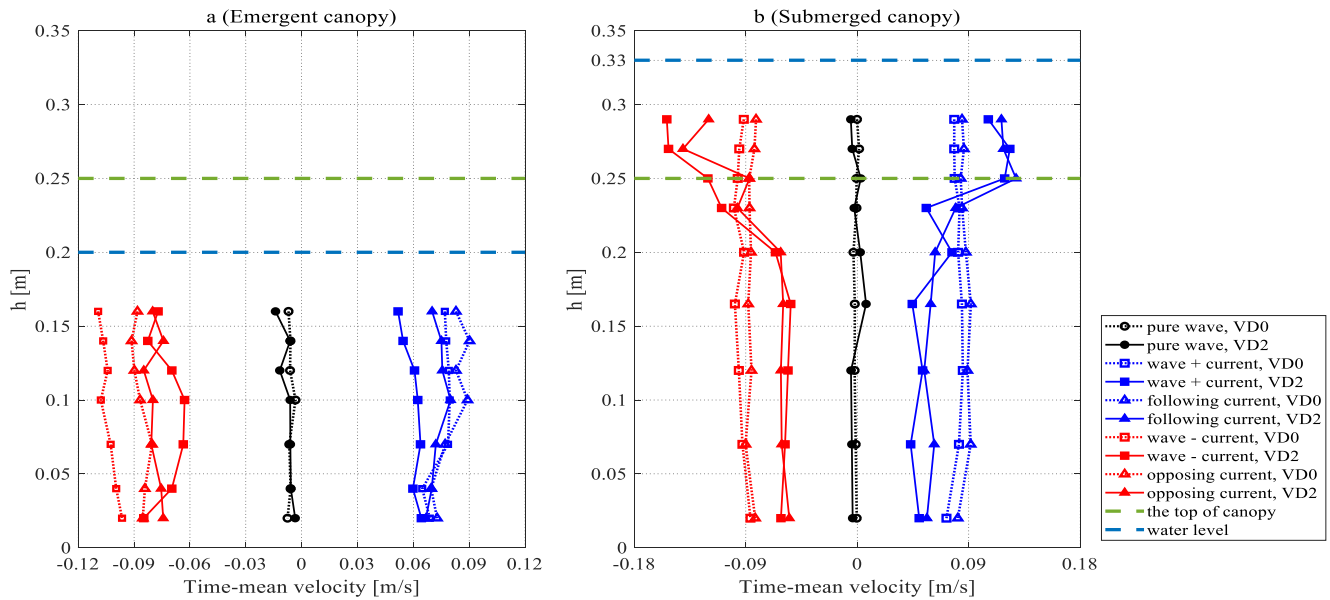


**Figure 2.** Vertical profile of time averaged velocity in (a) emergent and (b) submerged VD2 canopies. In both cases, the incident wave height, wave period and imposed current velocity is 5 cm, 0.8 s and  $\pm 0.09$  m/s, respectively.

creating steady opposing currents. The intended water depths (e.g.,  $h = 0.33$  cm) were achieved with ca. 1-cm offset. In each test, the wavemaker was started after steady flow and still water surface was achieved. To test the possible influence of mimic spatial arrangement, both regularly and randomly arranged canopies were tested in the present experiment (Figure S1 in Supporting Information S1).

The spatial wave height changes were measured by seven capacitance-type wave gauges (Figure 1c). In each test, velocity was measured by three Nortek ADVs (acoustic doppler velocimeter) at halfway of the water depth with a sampling frequency of 50 Hz. The period-averaged velocities were based on time series of at least three wave periods. Considering the two water depths and the canopy height in our experiment, the measured velocity at this vertical position can be regarded as the averaged in-canopy velocity (Z. Hu et al., 2014, see Figure 2). Amplitude of the horizontal wave orbital velocity is  $U_w = (U_{max} - U_{min})/2$ , where  $U_{max}$  and  $U_{min}$  are the measured peak flow velocities in the positive and negative directions in a wave period at the middle of the water column. Imposed current velocity  $U_c$  is the time-averaged velocity at halfway of the water depth before waves were generated. In selected tests (i.e., 5 cm wave height and 0.8 s wave period with different current velocities), velocity profiles were measured by changing the vertical position of the ADV probes in repeated runs. The accuracy of ADVs was  $\pm 0.5\%$ . Their data were recorded only when the signal-to-noise ratio was higher than 15 dB, and correlation was higher than 80%.

Force sensors were installed at the same cross-section of the above-mentioned velocity measurements to compose a synchronized force-velocity measuring system for drag coefficient derivation (Figure 1c, see Yao et al., 2018). The force sensors were model M140 made by UTILCELL, whose accuracy is  $\pm 0.017\%$  (<https://www.utilcell.com/en/load-cells/load-cell-m140>). These sensors were also measured at 50 Hz and were hidden in the false bottom to avoid disturbance of the flow. Three individual rods were firmly attached to these sensors by screws. These force sensors were calibrated by adjusting their output with known weights. The output of the sensors is the total force acting on the testing rod, regardless the location of the acting force. These measuring rods were put on the centerline of the flume, and the ADVs were placed 5 cm apart at the same cross-section. A few mimics were removed to accommodate the synchronized force-velocity measuring system. This system was only applied for regular canopies but not for random canopies, in which flow in the cross-section is nonuniform. The output of these sensors is weight and can be easily converted to force. The output value would not change with the acting position on the measuring rod.

In total, 366 tests were conducted. Each test has a unique set of stem density, stem arrangement, submergence, and current-wave combinations (Table 1). To ensure repeatability, each test was repeated three times. For simplicity,

**Table 1**  
*Test of Regular Canopies With Different Hydrodynamic Conditions*

Water depth ( $h$ )/ plant height ( $h_v$ ) [-]	Mimic stem density (N) [stems/m <sup>2</sup> ]	Volumetric frontal area ( $a$ ) [m <sup>-1</sup> ]	Wave height ( $H$ ) [m]	Wave period ( $T$ ) [s]	Wave case name	Current direction and velocity ( $U_c$ ) [m/s]	$Re$ [-]	$\alpha (U_c/U_w)$ [-]
0.20/0.25	139/556	1.39/5.56	0.03	0.6	Wave0306 <sup>a</sup>	0/±0.03/±0.06/±0.09/±0.12/±0.15	[232, 1,992]	[-2.64, 2.77]
			0.03	0.8	Wave0308	0/±0.03/±0.06/±0.09/±0.12/±0.15	[429, 2,088]	[-3.09, 2.03]
			0.05	1.0	Wave0506	0/±0.03/±0.06/±0.09/±0.12/±0.15	[353, 2,190]	[-1.12, 1.78]
			0.05	0.8	Wave0508	0/±0.03/±0.06/±0.09 <sup>b</sup> /±0.12/±0.15	[550, 2,389]	[-2.02, 1.23]
			0.05	1.0	Wave0510	0/±0.03/±0.06/±0.09/±0.12/±0.15	[815, 2,623]	[-1.38, 1.04]
0.33/0.25	139/556	1.39/5.56	0.03	0.6	Wave0306	0/±0.03/±0.06/±0.09/+0.12/+0.15	[175, 1,526]	[-1.73, 4.80]
			0.03	0.8	Wave0308	0/±0.03/±0.06/±0.09/+0.12/+0.15	[346, 1,475]	[-1.50, 2.86]
			0.05	1.0	Wave0506	0/±0.03/±0.06/±0.09/+0.12/+0.15	[334, 1,564]	[-0.67, 3.38]
			0.05	0.8	Wave0508	0/±0.03/±0.06/±0.09/+0.12/+0.15	[539, 1,783]	[-1.03, 1.81]
			0.05	1.0	Wave0510	0/±0.03/±0.06/±0.09/+0.12/+0.15	[741, 1,850]	[-0.82, 1.26]
			0.07	0.8	Wave0708	0/±0.03/±0.06/±0.09/+0.12/+0.15	[777, 1,956]	[-0.72, 1.21]
			0.07	1.0	Wave0710	0/±0.03/±0.06/±0.09/+0.12/+0.15	[944, 2,126]	[-0.55, 0.93]

<sup>a</sup>The name of the wave case contains the information of wave height (0.03 m) and wave period (0.6 s). <sup>b</sup>These tests contain detailed velocity profile measurements. “+” means current flow in the same direction of waves, “-” means current flow in the opposite direction of waves.

we only tested regular waves, but they are nonlinear as Stokes drift can be observed. The wave height ranged from 0.03 to 0.07 m, and the wave period ranged from 0.6 to 1.0 s. The tested wave heights were selected so that the wave crests were consistently below the top of the emergent canopy and the wave troughs were always above the submerged canopy top. In the flume, we created waves with the steady following (positive) and opposing (negative) currents with reference to the direction of wave propagation. The default input waves from the wavemaker would have different wave heights at the canopy front due to the influence of underlying following and opposing currents. To simulate field conditions with the same incident wave height but different underlying current velocities, we adjusted the inputs of the wavemaker to ensure the wave height arriving at the canopy front is constant (within 5%) in various flow conditions (Z. Hu et al., 2014).

In the following current cases, current velocity varied from zero (pure wave case) to 0.15 m/s. In opposing current cases, velocities higher than 0.09 m/s led to unstable water surfaces. Thus, these tests were excluded from the experiment. The achieved velocity ratio ( $\alpha = U_c/U_w$ ) is in the range of [-2.4]. To avoid the possible influence of wave reflection, we only used the data of the first three to five waves with desired wave height in the analysis (Z. Hu et al., 2014). Lastly, the obtained data are analyzed collectively with previous experiments with the following currents (Z. Hu et al., 2014). In the experiment of Z. Hu et al. (2014), the tested following current velocity ranged from 0 to 0.3 m/s. The tested wave height and wave period were 0.04–0.2 m and 1–2.5 s, respectively. The tested water depths were 0.25 and 0.5 m. The obtained velocity ratio ( $\alpha = U_c/U_w$ ) was in the range of [0.5, 2].

## 2.2. A Direct Method of Deriving $C_D$ With Coexisting Currents

The obtained synchronized force-velocity data were used to obtain  $C_D$  directly based on the original Morison equation (Morison et al., 1950):

$$F = F_D + F_M = \frac{1}{2} \rho C_D h_v b_v u(t) |u(t)| + \frac{\pi}{4} \rho C_M h_v b_v^2 \frac{\partial u(t)}{\partial t} \quad (1)$$

where  $F$  is the total force,  $F_D$  is the drag force [N],  $F_M$  is the inertial force [N],  $u(t)$  is the instantaneous in-canopy velocity in the horizontal direction, equals to  $U_{in} + U_w \sin(\omega t)$ , where  $U_{in}$  is the time-averaged depth-averaged current velocity in the canopy with coexisting waves. Note that  $U_{in} \neq U_c$ , which is imposed time-averaged velocity without wave influence.  $\rho$  is the fluid mass density [kg/m<sup>3</sup>],  $h_v$  is the height of vegetation in water [m],  $b_v$  is the plant stem diameter [m].  $C_D$  and  $C_M$  are the drag coefficient [-] and inertia coefficient [-], respectively.  $C_M$  equals 2 for circular cylinders (Dean & Dalrymple, 1991; Nepf, 2011). Synchronized force-velocity data is critical for

$C_D$  quantification, but small time lags exist between the  $F_D$  and  $u$  time-series due to small misalignments between the two measuring probes and/or the intrinsic delays of the electronics. With the measured data of  $F$  and  $u$ , we calculated the time-series of  $F_D$  by Equation 1. Then, time lags can be obtained by comparing the peaks of the  $F_D$  and  $u$  signals. Subsequently,  $F$  time-series is adjusted to eliminate the time lags and used in the next run. This loop was executed over 30 times by an automatic script and the minimum time lag was then chosen to derive  $C_D$ . More details on the signal realignment can be found in Yao et al. (2018) and the minimum time lag is in the order of 0.001 s. The realigned data of  $F$  and  $u$  can be used to derive instantaneous  $C_D$  using Equation 1 (see Figure S2 in Supporting Information S1), but period-averaged  $C_D$  is more relevant in WDV quantification (see Equation 2).

Note that  $F_M$  does not contribute to WDV, as the work done by  $F_M$  in a wave period is zero (Dalrymple et al., 1984). This holds for both pure wave and combined current-wave flows. Therefore, the work done by  $F$  in a wave period is equal to that done by  $F_D$ , and a period-averaged  $C_D$  can be obtained as in Z. Hu et al. (2014) and H. Chen et al. (2018):

$$C_D = \frac{2 \int_0^T F_D u(t) dt}{\int_0^T \rho h_v b_v u^2(t) |u(t)| dt} = \frac{2 \int_0^T F u(t) dt}{\int_0^T \rho h_v b_v u^2(t) |u(t)| dt} \quad (2)$$

By using this equation, we can obtain a period-averaged  $C_D$  based on the actual contribution to the WDV via considering the work done by  $F$ , and prevent the possible errors related to the instantaneous  $C_D$  that may reach unrealistically high values when  $F_D$  is divided by very small velocity in Equation 1. A spatial mean  $C_D$  is obtained by averaging the values from three locations in the flume.

### 2.3. WDV Data Analysis

Wave height attenuation induced by a unit length of canopies is expressed as (Z. Hu et al., 2014; Paul et al., 2012):

$$\Delta H = \frac{H_0 - H_{out}}{L} \quad (3)$$

where  $H_0$  and  $H_{out}$  is the wave height at the front and the end of a vegetated area [m], respectively.  $L$  is the length of the vegetated area [m]. The wave height reduction in canopies was subtracted by the wave height reduction measured in the control test (VD0), so that the effect of flume bed and sidewall friction is excluded.

To quantify the effect of imposed currents on WDV, the relative wave height decay  $r_w$  [-] in current-wave and pure wave flows is defined as (Z. Hu et al., 2014):

$$r_w = \frac{\Delta H_{cw}}{\Delta H_{pw}} \quad (4)$$

Subscript “*pw*” and “*cw*” indicate pure wave and combined current-wave conditions. To reveal the impact of currents in the upper free layer on WDV, we define a new parameter ( $\Delta R$  [-]) to show the difference of relative wave height attenuation in emergent and submerged canopy:

$$\Delta R = \frac{(H_0 - H_{out})_{em} - (H_0 - H_{out})_{sub}}{H_0} \quad (5)$$

Subscript “*em*” and “*sub*” stand for emergent canopy and submerged canopies, respectively.

### 2.4. Modeling of Direct WDV

Direct WDV is originated from vegetation drag, whereas the indirect WDV accounts for the wave height reduction due to wave breaking, which is indirectly linked to the drag. The direct WDV was considered in all the cases: submerged and emergent canopies in pure wave, and wave with both following and opposing currents. The indirect WDV was only considered in cases of submerged canopies with opposing currents, since wave breaking was only observed in these cases.

**Table 2**  
A Summary of Mean Current Velocity Inside and Above Canopy From Literature<sup>a</sup>

Source	Vegetation mimics	Flow condition	Volumetric frontal area (a) [m <sup>-1</sup> ]	Water depth (h)/plant height (h <sub>v</sub> )	Imposed current velocity, U <sub>c</sub> [m/s]	Mean velocity inside canopy, U <sub>in</sub> [m/s]	Mean velocity above canopy, U <sub>up</sub> [m/s]	U <sub>up</sub> /U <sub>in</sub>
Nepf and Vivoni (2000)	Plastic mimics	Current	2.11	0.44/0.16	0.1	0.045	0.12	2.7
López and Garcia (2001)	Rigid cylinders	Current	1.09	0.34/0.12	0.59	0.362	0.63	1.7
Z. Liu et al. (2012)	Shrubbery	Current	1.72	0.45/0.28	0.18	0.11	0.39	3.5
Huai et al. (2019)	Meadow model plant	Current	1.62	0.33/0.21	0.11	0.05	0.177	3.5
Shin et al. (2020)	Acrylic cylinders	Current	2.97	0.25/0.1	0.10	0.04	0.125	3.1
Z. Hu et al. (2014)	Stiff wooden cylinders	Wave with following current	5.56	0.50/0.36	0.15	0.079	0.27	3.4
M. Chen et al. (2020)	Stiff wooden cylinders	Wave with following current	1.34	0.8/0.4	0.25	0.071	0.24	3.4
Present study	Rigid cylinders	Wave with opposing current	1.39	0.33/0.25	-0.09	-0.05	-0.125	2.5

<sup>a</sup>Some of the listed studies contain more than one velocity profiles, in which we only select one of them as an example.

Our model of the direct WDV is modified from previous studies (Dalrymple et al., 1984; Z. Hu et al., 2014; Longuet-Higgins & Stewart, 1961; Losada et al., 2016). The model is based on the following assumptions:

1. Current velocities in and above canopies are both uniform vertically, noted as  $U_{in}$  and  $U_{up}$ , respectively; the  $U_{up}/U_{in}$  ratio is constant;
2. Current and wave velocities are uniform along the flume;
3. linear wave theory is applicable;
4. current and waves are collinear;
5. turbulent velocity fluctuations are neglectable; and
6. drag coefficient is a constant coefficient in space.

Assumption 1 is made following previous studies on submerged canopies (Lowe et al., 2005; Nepf, 2011). Assumption 2 is made for simplicity as our model aims to help to understand WDV variation rather than accurate prediction. It is noted that the ratio between the two velocities varies with water depth, imposed current velocity, vegetation type, and so on. (see Table 2). We used a constant ratio (i.e., 2.5) for all the cases, which was determined by averaging measured velocity profiles (Figure 2), and it is within the range of previously reported ratios (Table 2). Assumptions 3–6 were made following two previous models (Z. Hu et al., 2014; Losada et al., 2016). Vegetation-generated turbulence is important, but it would be too complex for our sample model to involve detailed quantification of turbulence. Its effect is lumped into the onset of wave breaking in Equation 18. The assumption of neglecting turbulent velocity fluctuations has been made in previous analytical models for WDV in combined current-wave flows as well (e.g., Losada et al., 2016).

For emergent canopies, the expression of the energy balance for waves with a steady current  $U$  can be given following Longuet-Higgins and Stewart (1961):

$$\frac{\partial}{\partial x}[E(c_g + U) + S_x U] = -\epsilon_{cw,w} \quad (6)$$

where  $E = \frac{1}{8} \rho g H^2$  is the wave energy density,  $H$ ,  $U$ ,  $C_g$ , and  $S_x$  is wave height, depth-averaged velocity of the whole water depth, wave group velocity, and radiation stress, respectively. Note that for emergent canopy,  $U$  is equal to  $U_{in}$ , whereas for submerged canopy,  $U$  is the averaged velocity of both layers considering their respective water depth. The subscript  $x$  indicates the direction of the wave propagation. The first term on the left of Equation 6 represents the transfer of wave energy by the wave group velocity plus the uniform velocity. The second term ( $S_x U$ ) represents the work done by the current  $U$  against radiation stress ( $S_x = E(2c_g/c - 1/2)$ , where  $c$  is wave celerity (Longuet-Higgins & Stewart, 1960, 1961). As  $U$  is uniform in the flow direction (Assumption 2),  $\partial U/\partial x = 0$  and thus the second term vanishes in Equation 6. In Equation 6,  $\epsilon_{cw}$  is drag-induced time-averaged energy dissipation rate for wave per unit horizontal area in combined currents-wave flows.  $\epsilon_{cw}$  and  $\epsilon_{cw,c}$  are



drag-induced energy dissipation rate for wave-current combination and for current, respectively. Following Li and Yan (2007),  $\epsilon_{cw} = \epsilon_{cw-w} + \epsilon_{cw-c}$ .

In pure wave conditions, time-averaged energy dissipation rate ( $\epsilon_{pw}$ ) can be derived as (Dalrymple et al., 1984; Méndez & Losada, 2004):

$$\epsilon_{pw} = \frac{2}{3\pi} \rho C_{D-pw} b_v N_v \left( \frac{kg}{2\sigma} \right)^3 \frac{\sinh^3 kh_v + 3\sinh kh_v}{3k \cosh^3 kh} H^3 \quad (7)$$

where  $k$  and  $\sigma$  is the wave number and wave angular frequency.  $N_v$  is the vegetation stem density.  $C_{D-pw}$  is obtained via an empirical relation with Reynolds number (see Equation 23 in Section 3.2), that is,  $Re = [|U_{max}|, |U_{min}|]_{max} b_v / \nu$ , where  $U_{max}$  and  $U_{min}$  are the measured maximum velocity in positive and negative direction within a period and  $\nu = 10^{-6} m^2/s$  is the kinematic viscosity (Z. Hu et al., 2014; Zhao et al., 2021).

$\epsilon_{cw-w}$  is a function of  $\epsilon_{pw}$ , following Z. Hu et al. (2014):

$$\epsilon_{cw-w} = f(\alpha) \epsilon_{pw} \quad (8)$$

where  $f(\alpha)$  is the ratio between  $\epsilon_{cw-w}$  and  $\epsilon_{pw}$ , considering nonlinear wave-current interaction in drag-induced dissipation. Following Assumptions 1 and 2,  $\epsilon_{pw}$  and  $\epsilon_{v-pw}$  can also be expressed as the time-averaged work done by the drag force:

$$\epsilon_{pw} = \frac{\omega}{2\pi} \int_{-\pi/\omega}^{\pi/\omega} N_v F_D U_w \sin(\omega t) dt = \frac{2}{3\pi} N_v \rho C_{D-pw} h_v b_v |U_w| U_w^2 \quad (9)$$

$$\begin{aligned} \epsilon_{cw-w} = \epsilon_{cw} - \epsilon_{cw-c} &= \frac{\omega}{2\pi} \int_{-\pi/\omega}^{\pi/\omega} N_v F_D (U_c + U_w \sin(\omega t)) dt - \frac{1}{2} N_v \rho C_{D-cw} h_v b_v |U_c| U_c^2 \\ &= \begin{cases} \frac{1}{2\pi} N_v \rho C_{D-cw} h_v b_v \left[ \sin^{-1} \left( \frac{|U_c|}{U_w} \right) (2|U_c| U_c^2 + 3|U_c| U_w^2) + \frac{1}{3} (4U_w^2 + 11U_c^2) \sqrt{U_w^2 - U_c^2} - \frac{1}{\pi} |U_c| U_c^2 \right], & |U_c| < U_w \\ \frac{1}{4} N_v \rho C_{D-cw} h_v b_v (2|U_c| U_c^2 + 3|U_c| U_w^2 - 2|U_c| U_c^2), & |U_c| \geq U_w \end{cases} \end{aligned} \quad (10)$$

Then,  $f(\alpha)$  is expressed as:

$$f(\alpha) = \frac{\epsilon_{cw} - \epsilon_{cw-c}}{\epsilon_{pw}} = \begin{cases} D \left( \frac{3}{4} \sin^{-1}(|\alpha|) (2|\alpha|\alpha^2 + 3|\alpha|) + \frac{1}{4} (4 + 11\alpha^2) \sqrt{1 - \alpha^2} - \frac{3\pi}{4} |\alpha|\alpha^2 \right) & |\alpha| < 1 \\ D \left( \frac{9\pi}{8} |\alpha| \right) & |\alpha| > 1 \end{cases} \quad (11)$$

where  $D = C_{D-cw}/C_{D-pw}$  is the ratio of  $C_D$  in combined currents-wave flow and pure wave cases. It should be noted that  $D$  varies in each case, a generic  $C_D-Re$  relation (Equation 23) for various current-wave combinations is needed to determine  $D$ . In pure wave tests, we observed a non-zero mean velocity in the opposite direction of the wave propagation, suggesting a weak recirculation current in the flume. This recirculation has also been observed in previous experiments, and it was attributed to Stokes drift (Z. Hu et al., 2014; Hudspeth & Sulisz, 1991). Additionally, similar to the experiment in Z. Hu et al. (2014) and M. Chen et al. (2020), we found that current velocity is suppressed due to wave motion: acting in-canopy velocity  $U_{in}$  in combined current-wave flow is smaller than the imposed velocity current without wave influence, that is,  $U_c$ . To account for these effects, two modifications to Equation 8 are made following the Z. Hu et al. (2014): (a) in pure wave cases, time averaged in-canopy velocity ( $U_{in}$ ) is non-zero and in the negative direction,  $U_{in}/U_w = -0.04$ , which is determined by averaging the ratios of all the pure wave cases; (b) in current-wave cases, current velocity is found suppressed by wave motions (i.e., see Figure 2). It is likely due to the fact that the bidirectional orbital velocity by wave motion forms addition obstacle to the unidirectional flow. For following current cases,  $|U_{in}/U_w| - |U_c/U_w| = -0.13$ , whereas for opposing current cases,  $|U_{in}/U_w| - |U_c/U_w| = -0.03$ , in which  $U_{in}$  and  $U_c$  represent the magnitudes of the current velocity with and without wave presences. These values were obtained by averaging all the cases with regular canopies. Subsequently,  $f(\alpha)$  is modified as:

$$f'(\alpha) = \begin{cases} 1 & \alpha = 0 \\ \frac{f(|\alpha| - 0.13)}{f(-0.04)} & \alpha > 0 \\ \frac{f(|\alpha| - 0.03)}{f(-0.04)} & \alpha < 0 \end{cases} \quad (12)$$

Substituting equations of  $E$ ,  $S_x$  and Equation 8 into Equation 6 and replacing  $f(\alpha)$  with  $f'(\alpha)$ , Equation 6 can be rewritten below (see Text S1 in Supporting Information S1 for the deviation process), following a similar form as Equation 48 in Dalrymple et al. (1984):

$$\frac{\partial H^2}{\partial x} = -A_0 H^3 \quad (13)$$

$$A_0 = f'(\alpha) \frac{8\varepsilon_{v-pw}}{\rho g \left[ (c_g + U) + U \left( \frac{2kh}{\sinh(kh)} + \frac{1}{2} \right) \right]} H^3 \quad (14)$$

Solving the differential equation (Equation 13) with the boundary condition that the wave height at the starting edge of the vegetation field is  $H(x = 0) = H_0$ , the wave height along the canopy (at distance  $x$ ) can be derived as (Dalrymple et al., 1984; Méndez & Losada, 2004, see also Text S1 in Supporting Information S1):

$$H_x = \frac{H_0}{1 + \beta x} = K_v H_0 \quad (15)$$

where  $K_v$  is the relative wave height and  $\beta$  is the damping factor:

$$\beta = \frac{A_0 H_0}{2} \quad (16)$$

## 2.5. Modeling of Indirect WDV by Wave Breaking

Until Equation 16, we only considered the direct WDV by drag force following previous works (Dalrymple et al., 1984; Z. Hu et al., 2014; Longuet-Higgins & Stewart, 1961; Losada et al., 2016). Next, we will consider the additional indirect WDV by current-induced wave breaking ( $\varepsilon_b$ ), which is a new extension to the WDV modeling. The conservation of wave energy flux equation Equation 6 is then modified as:

$$\frac{\partial}{\partial x} [E (c_g + U) + S_x U] = -\varepsilon_{cw-w} - \varepsilon_b \quad (17)$$

where the term related to radiation stress  $S_x \partial U / \partial x$  is excluded as Assumption 2 still holds for submerged cases.  $U$  is now the depth-averaged velocity for both layers.  $\varepsilon_{cw-w}$  is the same as the emergent canopy in Equation 6.  $\varepsilon_b$  is the time-averaged rate of energy dissipation per unit horizontal area, which only exists in cases of opposing currents. Wave breaking occurs when steepness exceeds the Miche's steepness limited criterion following (Chawla & Kirby, 2002):

$$\frac{k_{cw} H_b}{\gamma \tanh k_{cw} h} \geq 1 \quad (18)$$

where  $k_{cw} = 2\pi / [T(c_g + U_{up})]$  is the wave number considering currents in the upper free layer,  $\gamma$  is a dimensionless parameter that determines the onset of wave breaking.  $H_b$  is the critical breaking wave height. For a specific case, we put the data from the experiments into Equation 18 to determine if breaking occurs.

Subsequent to the onset, the expression of  $\varepsilon_b$  can be given following an analogy of bore dissipation (Battjes & Janssen, 1978):

$$\varepsilon_b = \frac{\theta}{8\pi} \rho g k_{cw} \sqrt{g/h} H^3 \quad (19)$$

where  $\theta$  is a nondimensional parameter which relates  $\varepsilon_b$  to energy dissipation in breaking waves. Though the bore model was derived for depth-limited wave breaking, the same expression has been used in determining energy dissipation by current-limited wave breaking (Chawla & Kirby, 2002). The contribution of wave breaking to the total wave dissipation can be assessed by comparing  $\varepsilon_b$  to the sum of  $\varepsilon_{cw,w}$  and  $\varepsilon_b$ .

Taking  $\varepsilon_b$  into account, Equation 17 can be rewritten as the following form (see Text S2 in Supporting Information S1 for the derivation process):

$$\frac{\partial H^2}{\partial x} = -(A_0 + B_0) H^3 \quad (20)$$

where  $B_0 = \frac{8\varepsilon_b}{\rho g \left[ (c_g + U) + U \left( \frac{2kh}{\sinh(kh) + \frac{1}{2}} \right) \right] H^3}$  is related to wave breaking in opposing currents, and  $A_0$  is related to vegetation drag force as in Equation 12. By solving Equation 20, the wave height along the canopy can be derived as (see Text S2 in Supporting Information S1)

$$H_x = \frac{H_0}{1 + (\beta + \lambda)x} \quad (21)$$

$$\lambda = \frac{B_0 H_0}{2} \quad (22)$$

where  $\beta$  and  $\lambda$  are related to vegetation drag and wave breaking, respectively. Chawla and Kirby (2002) set parameters  $\gamma$  and  $\theta$  as 0.6 and 0.1 to explain the energy dissipation of a flume experiment. In our study,  $\gamma$  and  $\theta$  were determined by calibration, that is, tuning these parameters to obtain the best fit against observed WDV (Zheng et al., 2008). Specifically,  $\gamma$  and  $\theta$  were 0.7 and 0.05 for low vegetation density cases (VD2), and 0.4 and 0.3 for high vegetation density cases (VD3).

### 3. Results

#### 3.1. Velocity Profiles Within and Above Vegetation Canopy

As WDV is closely related to the velocity structure of combined current-wave flows, detailed vertical velocity profiles of different conditions were measured in wave0508 test as an example (Figure 2). The observed velocity profiles show that the existence of vegetation has a large impact on the velocity profiles in both submerged and emergent canopies. In the emergent canopies, the effect of vegetation is mainly reducing the current velocity, as the time-averaged velocity is lower in tests with vegetation compared to the control tests (Figure 2a). In submerged canopies, vegetation reduces the in-canopy velocity and diverts currents to the upper free zone, leading to a distinctive shear layer (Figure 2b). A shear layer exists in all tests with currents (i.e., pure current and combined current-wave cases). On average, the time-averaged velocity magnitude in the upper free zone was about 2.5 times the in-canopy velocity (Figure 2b). Such velocity ratio is adapted in WDV modeling in Sections 2.4 and 2.5. It is further noticed that time averaged velocity in pure wave cases is not zero. When comparing the pure current cases with current-wave cases (Figures 2a and 2b), the existence of waves can reduce the velocity magnitude regardless of the current direction. These two points lead to modifications of the direct WDV modeling (Equation 12) similar to that in Z. Hu et al. (2014).

#### 3.2. $C_D$ in Following and Opposing Currents

To apply the direct measuring method to derive  $C_D$ , simultaneous velocity and force data were collected in all tests with various current-wave combinations (Z. Hu et al., 2020). In addition to previous studies, we now include simultaneous velocity, force and  $C_D$  when waves propagate with opposing currents (Figure S3 in Supporting Information S1). Based on the simultaneous velocity-force data, period-averaged  $C_D$  values were derived. The extension to previous studies is that we now reveal  $C_D$  variation with  $Re$  in cases of opposing currents based on the direct measuring method (Figure 3). The tested  $Re$  number ranges from 200 to 2,600. It shows that in all the cases (pure wave and wave  $\pm$  currents),  $C_D$  decreases with  $Re$  number. There is no apparent difference between the cases with opposing current comparing to other cases (Figures 3 and S3 in Supporting Information S1). The obtained  $C_D$  values are scattered when  $Re$  is between 200 and 1,500, but most data points are within the range

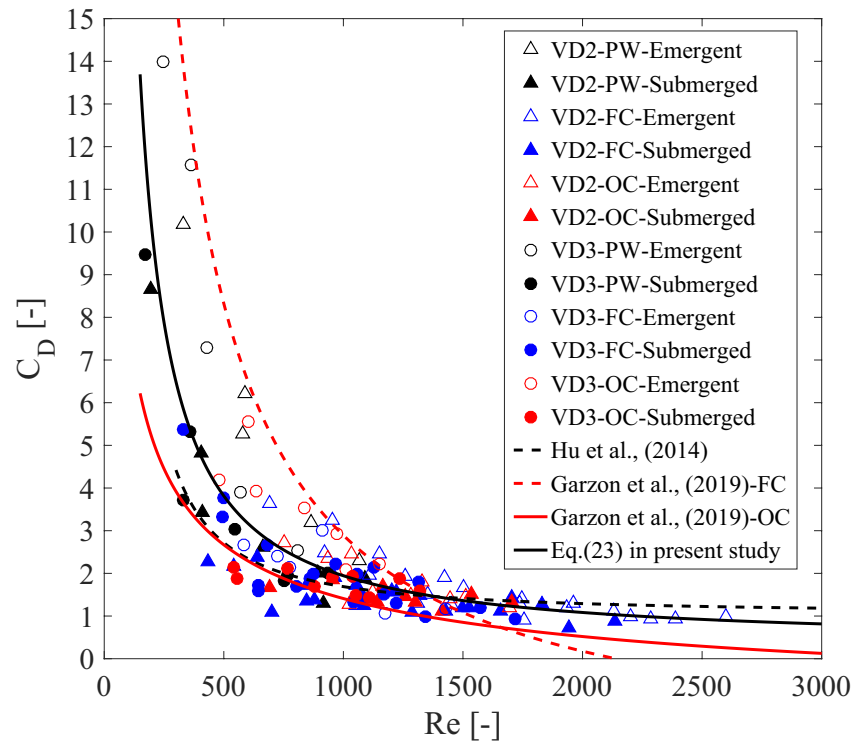


**Figure 3.** Relation between period-averaged  $C_D$  and  $Re$  number. The shown data are from all the tests with regular canopies in this study (Table 1). In random canopies, simultaneous velocity-force data were not collected, as flow in the cross-section is nonuniform and  $C_D$  cannot be directly derived.

described by the empirical relations in Z. Hu et al. (2014) for following currents and Garzon et al. (2019) for both following and opposing currents ( $C_D$  derived by calibration method). When  $Re$  is higher than 1,500, the obtained  $C_D$  approaches a constant value of 1.30, similar to Z. Hu et al. (2014) and Losada et al. (2016). Additionally, the difference between cases with different vegetation densities and submergence is insignificant as they all share a similar decreasing pattern with  $Re$  (Figures 3 and S3 in Supporting Information S1). Based on the current data set, we propose a new empirical  $C_D$ - $Re$  relation (Equation 23 and see Figure 3) covering different current-wave combinations and canopy conditions ( $R^2 = 0.68$ ). This relation is also similar to that in Z. Hu et al. (2014) but with additional coverage of opposing currents. The formation of the  $C_D$ - $Re$  relation is:

$$C_D = 0.35 + 3652Re^{-1.116} \quad (170 < Re < 2600) \quad (23)$$

This relation is applicable to emergent and shallowly submerged canopies ( $1 < h/h_v < 2$ ) with rigid stems. The usage of this relation for WDV and drag force assessment is further discussed in Section 4.1.

### 3.3. Wave Dissipation in Vegetation Canopy With Following and Opposing Currents

Our experiments have revealed diverse WDV variations with underlying currents (Figure 4). When the imposed following current velocity is small (i.e.,  $U_c = 0.03$  m/s,  $\alpha = 0.22$ ), WDV is reduced compared to the pure wave cases (Figure 4a). However, as following current velocity increases to 0.12 m/s (i.e.,  $\alpha = 0.98$ ), WDV becomes higher than the pure wave cases. WDV can be further increased with higher velocity (i.e., 0.15 m/s,  $\alpha = 1.21$ ). As a contrast, opposing currents can more easily enhance WDV than following currents (Figure 4a vs. Figure 4b). WDV increases immediately when a small opposing current is imposed (i.e.,  $U_c = -0.03$  m/s,  $\alpha = -0.29$ ). It further increases as the opposing velocity rises to  $-0.06$  m/s ( $\alpha = -0.49$ ) and  $-0.09$  m/s ( $\alpha = -0.72$ ). In such a test, the relative wave height ( $K_v$ ) reduction is close to 30%. Furthermore, it is worth noticing that the variation between repeated runs (i.e., error bars in Figures 4a and 4b) is small, indicating the repeatability of the results.

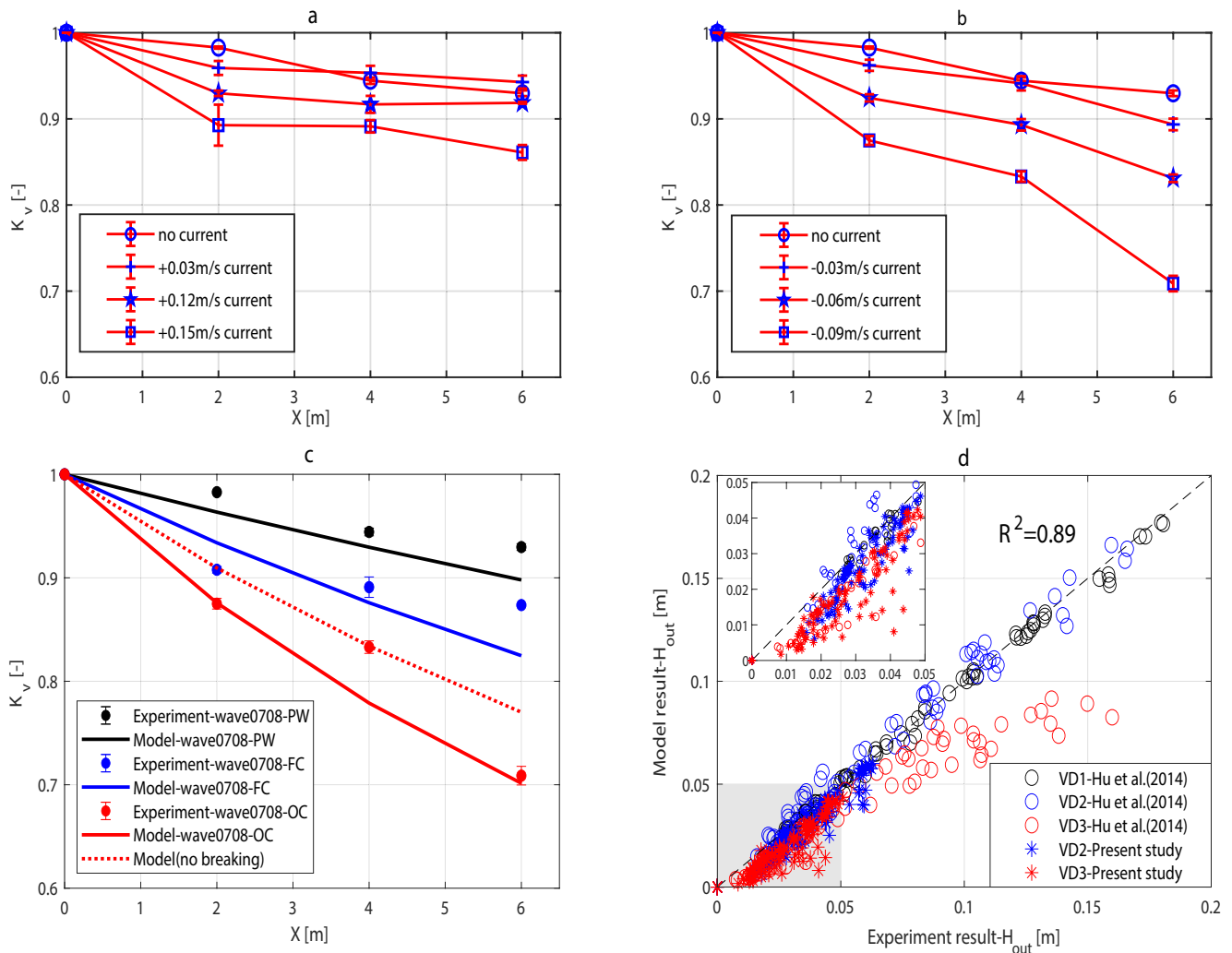


**Figure 4.** Relative wave height ( $K_v$ ) evolution in submerged regular canopies with (a) following currents and (b) opposing currents. (c) Modeled and measured  $K_v$  in the pure wave as well as the wave with following currents ("FC") and opposing currents ("OC"). (d) An overall comparison between modeled and measured wave height at the end of the vegetation canopy ( $H_{out}$ ) based on the data from the current experiment and from Z. Hu et al. (2014). The shaded area is enlarged in (d) to better show the data from the present experiments. In (a)–(c), the data points are the mean value of the repeated runs of one test, and the error bars are the standard deviations. The tested wave height is 7 cm and the wave period is 0.8 s. All the modeling results are derived from Equation 15, unless wave breaking is considered, in which case Equation 21 is applied instead.

The proposed new WDV model (Equations 15 and 21) agrees reasonably well with the measured wave height variations (Figure 4c). Similar to the experiments, the modeling results also show that opposing currents lead to greater WDV than following currents. Modeling results further show that WDV would be underestimated if current-induced wave breaking is not accounted for, indicating the importance of this process. In our experiment, wave (partial) breaking in opposing currents occurs when the ratio of imposed currents velocity  $U_c$  and the wave celerity ( $c$ ) exceeds 1/50 (see Movie S1 and Figure 1b), whereas wave blocking occurs when the ratio exceeds 1/10 (see Movie S2). An overall assessment of the model accuracy shows that our model can well reproduce the observed wave height at the end of the canopy ( $H_{out}$ ) from both Z. Hu et al. (2014) and the present experiments ( $R^2 = 0.89$ , Figure 4d). However, our model tends to underestimate  $H_{out}$ , that is, overestimate WDV, when vegetation stem density is high (VD3 cases). In cases with small  $H_{out} < 0.05$  m, where most of the current experiment data situated, the  $R^2$  value of the model is 0.62, which also has a clear underestimation trend. The reason for this trend is discussed in Section 4.3.

The variation of  $r_w$  with  $\alpha$  can systematically reveal the effect of underlying currents on WDV (Figure 5). Recall that  $r_w$  is the ratio of wave height decay in current-wave cases over pure wave cases. In the tests with following

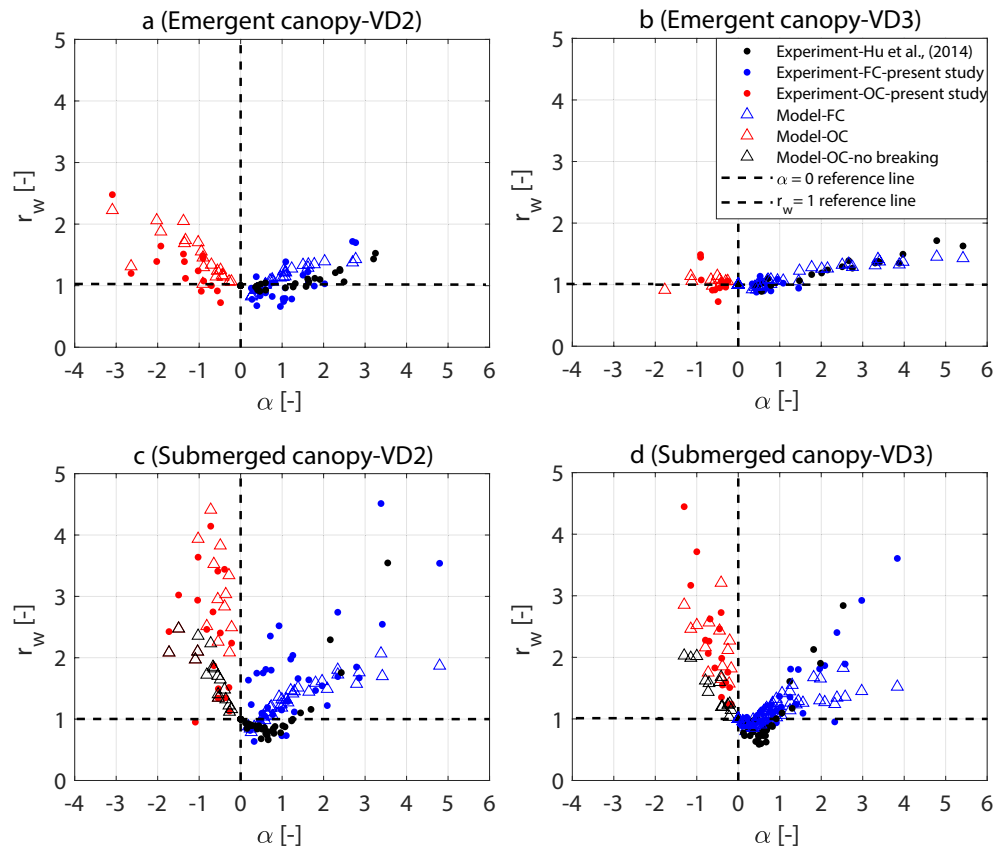


**Figure 5.** Variation of relative wave height decay ( $r_w$ ) with velocity ratio ( $\alpha$ ) in different submergence conditions and vegetation density. In the legend, “FC” means following currents, “OC” means opposing currents.

currents, WDV is reduced compared to pure wave tests (i.e.,  $r_w < 1$ ) when the imposed current velocity is smaller than the wave orbital velocity amplitude (i.e.,  $\alpha < 1$ ), but WDV can be increased when  $\alpha > 1$ . Comparing to tests with following currents, opposing currents ( $\alpha < 0$ ) lead to higher dissipation (higher  $r_w$ ), except for the cases with emergent high-density canopy (VD3). Possible reason for this variation is included in Section 4.2. Furthermore, the enhanced WDV by opposing currents is more apparent in submerged conditions than emergent conditions, as  $r_w$  rises more rapidly in submerged conditions (Figures 5c and 5d).

Our model shows an acceptable agreement (overall  $R^2 = 0.45$ ) with the observed  $r_w$  variation in the present experiments and the experiment in Z. Hu et al. (2014), although discrepancy between the model and experiments exists (Figure 5). The reason we provide prediction at each data point in Figure 5 is because that the developed model derives wave height along the canopy (see Equations 15 and 21), but it cannot directly derive the relative wave height decay ( $r_w = \frac{\Delta H_{cw}}{\Delta H_{pw}}$ ). Thus, for each data point, we use the derived wave height changes ( $\Delta H_{pw}$  and  $\Delta H_{cw}$ ) to calculate  $r_w$ , and an accurate prediction of  $r_w$  would require accurate results of both wave height changes. Discrepancy between modeled and measured  $r_w$  is anticipated since the role of the analytical model is to improve our understanding rather than providing precise predictions of the WDV variations. Importantly, this model shows (a) in following current cases,  $r_w$  first decreases and then increases with  $\alpha$ , and (b) in submerged cases, opposing currents promote dissipation much more quickly than following currents due to the additional indirect WDV, that is, wave breaking. With the help of the model, we show that if breaking is not accounted for in opposing current cases,  $r_w$  is underestimated (Figures 5c and 5d). These results indicate the importance of including current-induced breaking (i.e.,  $\epsilon_b$  in Equation 17). Additionally, our experiments further reveal that there is no apparent difference in  $r_w$  variations between the regular and random vegetation canopies. For details, please see Figure S4 in Supporting Information S1.

Since we only tested one submergence ratio and kept a constant ratio between  $U_{up}/U_{in}$ , we performed sensitivity analyses to show how these factors influence model output (Figure 6). As the increase of submergence ratio

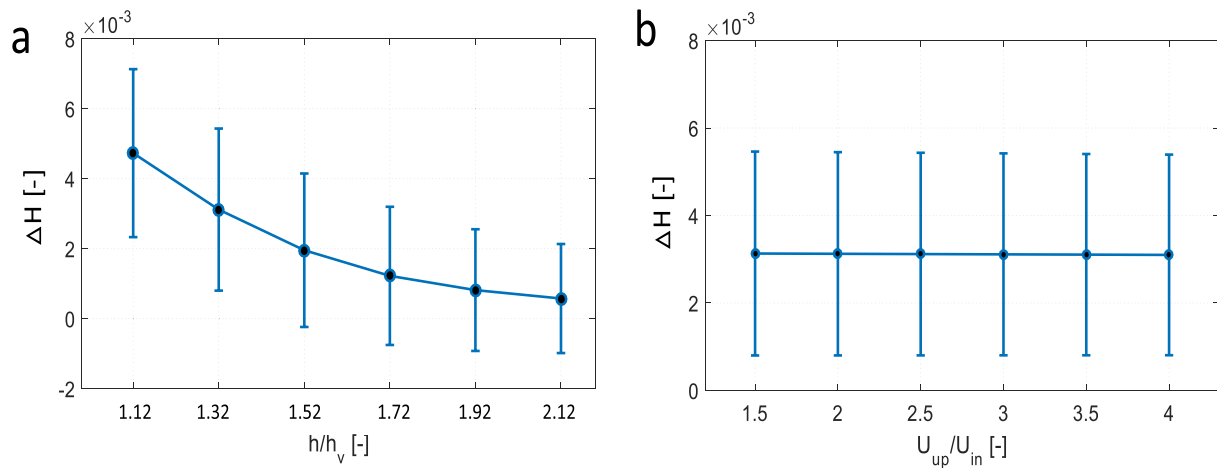


**Figure 6.** Sensitivity analysis of the submergence ratios ( $h/h_v$ ) and the velocity ratios ( $U_{up}/U_{in}$ ) on the modeled wave height attenuation per unit length ( $\Delta H$ ). This analysis is based on all the submerged cases. The points are mean values and the bars show the standard deviation.

(Figure 6a), the averaged wave height dissipation rate per unit length is reduced. Such a reduction is in-line with previous studies (e.g., Augustin et al., 2009), and it is likely induced by the reduced vegetation present in the higher water column, where strong wave orbital velocity exists. Contrastingly, if we change the applied velocity ratio ( $U_{up}/U_{in}$ ) in the model, the result  $\Delta H$  does not seem to change accordingly (Figure 6b).

Finally, we evaluate the difference in WDV between emergent and submerged canopies and its variation with underlying currents (Figure 7). Not surprisingly, our experiments show that WDV is higher in emergent canopies compared to submerged canopies ( $\Delta R > 0$ ) in all the tests, where  $\Delta R$  is the difference in relative wave height attenuation between emergent and submerged canopy. However, it is worth noticing that the difference between the two submergence conditions reduces as the underlying current velocity increases in either positive or negative directions. Such a reduction implies that enhanced wave-current interaction (in both directions) can compensate

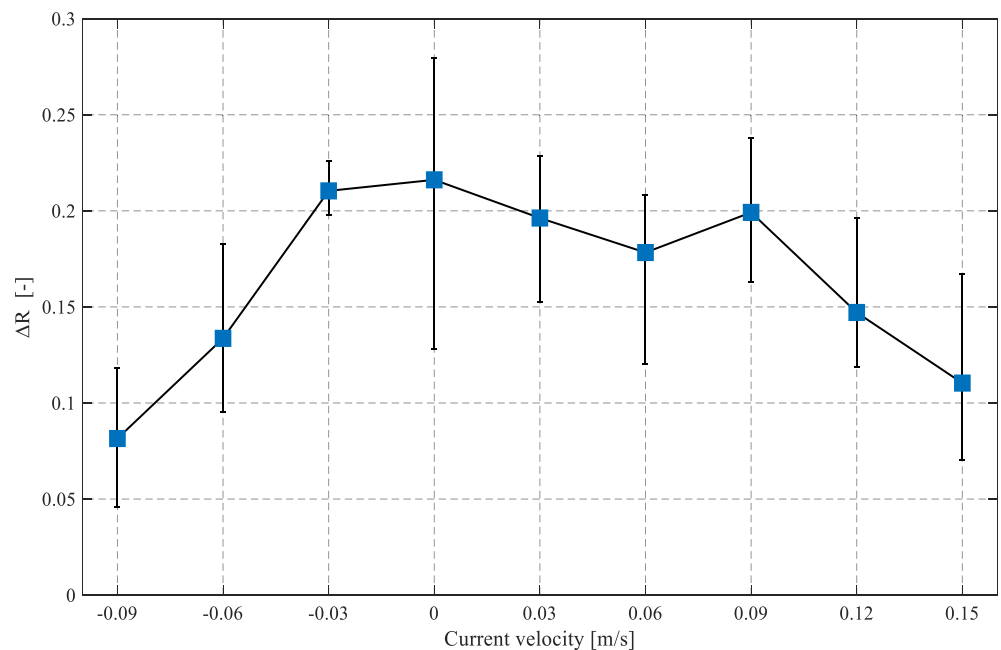


**Figure 7.** The difference of relative wave height attenuation in emergent and submerged canopy ( $\Delta R$ ) with following and opposing currents. The shown data are based on the present flume experiments not from modeling. The data points are the mean values of the various tests with different wave inputs but with the same imposed current (i.e., cases wave0306, wave0308, wave0506, wave0508, and wave0510), and the error bars show the standard deviations of these tests.

for the absence of vegetation area in the upper water column of submerged canopies. From our data set and modeling, there are 42 cases with submerged canopy in opposing currents, and wave breaking occurred in 73.8% of them. This percentage does not change during our sensitivity analysis (Figure 6). Once breaking occurred, it contributed 41%–87% of the dissipation. Current-induced breaking may eventually lead to an almost comparable wave height reduction as for the emergent canopies, that is,  $\Delta R < 0.1$  when the imposed opposing velocity reaches  $-0.09$  m/s. Our flume cannot generate stronger opposing currents than this, but they can be easily found in field conditions, which may bring  $\Delta R$  to even lower values.

## 4. Discussions

### 4.1. A Generic Drag Coefficient Relationship for Various Current-Wave Combinations

In the current study, we extend the application of this method to wave with opposing currents. We show that the variation of  $C_D$  with  $Re$  in such flow conditions does not significantly differ from other flow conditions, that is, pure wave and wave with following currents. All  $C_D$  values share a similar decreasing trend with  $Re$  number. Thus, a generic  $C_D$ - $Re$  relation (Equation 23) can be obtained to describe  $C_D$  changes in various current-wave combinations, which facilitates the determination of drag coefficient ratios ( $D = C_{D_{cw}}/C_{D_{pw}}$  in Equation 12) in WDV modeling.

The previously derived  $C_D$ - $Re$  relation based on direct method (Z. Hu et al., 2014) has been applied in numerous WDV modeling studies (e.g., Z. Hu et al., 2019; P. L.-F. Liu et al., 2015; Suzuki et al., 2019; van Veelen et al., 2021; Wang et al., 2015). The new relation is expected to assist future studies as well. The usage of the newly derived relation (Equation 23) and the one in Z. Hu et al. (2014) ( $C_D = 1.04 + (730/Re)^{1.37}$ ,  $300 < Re < 4700$ ) can be specified as: (a) both relations are limited to emergent and shallowly submerged canopies ( $1 < h/h_v < 2$ ) with rigid stems; (b) if  $Re$  number is in the range [170 2,600] and the case under consideration involve opposing currents, it is better to use Equation 23; (3) if  $Re$  number is in the range of [2,600 4,700] and the case does not involve opposing currents, it is then better to use the equation in Z. Hu et al. (2014); (d) if  $Re$  number is in the range [300 2,600], both equations can be used; (e) if the  $Re$  number is in the range [0 170] or above 4,700, neither of the two equations can be used and other suitable equations should be applied. In practice, one can assume  $C_D$  equals 1 or 1.30 to obtain a first estimation of the velocity. Subsequently, the known velocity can be applied to obtain a  $Re$  number and then a new  $C_D$  value via the  $C_D$ - $Re$  relation. This iteration continues until the changes in velocity and  $C_D$  values became very small, which can be easily achieved in numerical schemes.

Furthermore, as Equation 23 is derived based on the direct force measurement approach, it can be readily used to predict the maximum force experienced by vegetation in various flow conditions (H. Chen et al., 2018). Such prediction is of critical importance to assess the resistance of coastal vegetation ecosystems under storm conditions (Simard et al., 2019). It is worth noticing that  $C_D$  in the current study is averaged spatially across three locations in the canopy for simplicity, but the original data of  $F$  and  $u$  at each location is included in the open data set (Z. Hu et al., 2020) to facilitate further investigation on spatially varying forces. Finally, the current data set can also assist further investigations on the full variation of the  $C_D$  with changing submergence ratio and stem densities (e.g., via machine learning), as the derived Equation 23 does not account for all the variations in the current data set, especially when the  $Re$  is smaller than 1,000.

### 4.2. Indirect WDV by Wave Breaking in Opposing Currents

Our study shows that current-induced wave breaking can occur in upper free layers of submerged canopies, which is a key finding of the present studies. The comparison between the following and opposing currents further shows the importance of the breaking process. With following currents, the accelerated wave energy flux (via wave bunching, see also Equation 5) can also lead to indirect WDV. However, its contribution is smaller than current-induced wave breaking in opposing currents, which constitutes a significant part of the total WDV (41%–87%). Thus, the opposing currents can induce the observed higher WDV comparing to following currents. To our knowledge, the current-induced wave breaking process has not yet been reported in WDV studies, but it has been well investigated in previous experiments without vegetation (Chawla & Kirby, 2002; Chen & Zou, 2018; Yu, 1952; Zheng et al., 2008). The mimic vegetation canopy in our experiments is similar to the elevated flume bed in previous studies, for example, Zheng et al. (2008), in which currents are also forced to a smaller portion of



the water column and interact with waves. As wave breaking can greatly contribute to WDV, we think it is important to include this process in future assessment wave dissipation capacity of submerged vegetation canopies.

Depth-induced wave breaking has been observed in a saltmarsh field (Yang et al., 2012), and its contributions to wave dissipation and turbulence have been evaluated (Méndez & Losada, 2004; Pujol & Nepf, 2012). However, this breaking is initiated by depth limits rather than the vegetation's existence. Our experiments showed that due to the existence of vegetation, opposing currents were diverted into the upper water column and triggers wave breaking. Our model showed that wave breaking occurred when  $U/c$  reaches ca. 1/50, whereas Yu (1952) inferred that without vegetation canopy, wave breaking occurs when  $U/c$  reaches 1/7. The early occurrence of wave breaking can be attributed to the inherent high turbulence level of the velocity shear layer, which can more easily induce wave breaking than the flow in empty flumes (M. Chen et al., 2020; Nepf, 2012). Therefore, we argue that the current-induced wave breaking is a part of the overall WDV as indirect WDV, rather than an independent process, for example, depth-induced wave breaking.

In emergent canopies, wave breaking in opposing currents does not occur, in which vegetation drag is likely the controlling process. Still, higher dissipation with opposing currents can be found in emergent canopies, similar to Maza et al. (2015). The reason is due to less suppressed in-canopy mean velocity ( $U_{in}$ ) as shown in Equation 12, that is, opposing currents can more quickly move out of the low WDV range ( $|\alpha| - 0.03 \approx 0$ ) comparing to the following currents ( $|\alpha| - 0.13 \approx 0$ ). Notably, such difference is only apparent in emergent low-density canopy (VD2) but not in the high-density canopy (VD3). This may be due to the fact that the emergent high-density canopy can lead to very high WDV regardless of other factors. Thus, the influence of the current direction is not apparent.

### 4.3. Advantage and Limitations of the WDV Model

The purpose of the proposed model is to help understand the complex WDV process, including both direct and indirect portions. The main advantages of this analytical model are: (a) it provides an adequate assessment of the onset and contribution of wave breaking to WDV, as the overall  $r_w$  variation pattern (following vs. opposing, breaking vs. no breaking) can be well captured by it; (b) its simple structure helps to reveal the key physical mechanism without complex numerical modeling. We think that this model may pave the way for more sophisticated predictors of WDV in field conditions.

Due to the crude model assumptions, there are certain limitations that confine its application and precision. First, Nepf (2004) has defined three classes of canopy flow: unconfined flow ( $h/h_v > 10$ ); submerged flow ( $1 < h/h_v < 10$ ); and emergent flow ( $h/h_v = 1$ ). Our model may not be applicable in unconfined flows, in which vegetation canopies act as a bottom boundary to the whole flow (Nepf, 2004), and cannot divert current to initiate breaking. As for submerged flow ( $1 < h/h_v < 10$ ), and specially with  $h/h_v$  decreases (e.g.,  $< 4.5$ ), the discontinuity in drag creates a region of strong shear (Ghisalberti & Nepf, 2002), where current-wave interaction can be very active and current-induced wave breaking can be expected in cases with opposing currents. The variation of indirect WDV with submerged ratios needs further investigation, as only one submerged ratio ( $h/h_v = 1.32$ ) was tested in the present study.

Second, the velocity profile in real submerged canopies may differ from the model assumption (Assumption 1). The present model has assumed that velocity above and within canopies ( $U_{up}$  and  $U_{in}$ ) is uniform (Lowe et al., 2005; Nepf, 2011), and the ratio between the two velocities is constant as 2.5 based on the observed velocity profiles (Figure 2). This is obviously a simplified characterization of the velocity structures for various real canopies, since the  $U_{up}$  and  $U_{in}$  ratio varies with different submergence, current-wave combination, and vegetation flexibility (Nepf, 2004). A case-specific description of the velocity structure would improve the model accuracy, especially for the indirect WDV in the upper free zone. However, this simplification makes the analytical modeling possible, and we expected the general variation pattern of the indirect WDV would still hold with different  $U_{up}/U_{in}$  ratios listed in Table 2.

Third, the determination of the  $\gamma$  and  $\theta$  needs further investigation. These two calibration parameters determine the onsets and the intensity of wave breaking, respectively. For two vegetation stem densities, the calibrated values of  $\gamma$  and  $\theta$  are different. Other factors such as submergence ratio and individual stem diameter may also influence the values of these two calibration parameters, but it cannot be revealed in the current study due to limited conditions we tested in the experiments. Further exploration is needed with more testing conditions to reveal the changing

patterns of the two parameters. Finally, the overestimation of WDV in our model for high-density cases may be related to the neglected ‘sheltering effect’, which is typical in dense canopies (Mancheno et al., 2021). This effect takes place when downstream stems are exposed to the wake of upstream stems, and the contribution of each stem to WDV is reduced. Naturally, such reduction in WDV is more apparent in dense canopies with more stems, which may lead to the model overestimation for high-density cases.

#### 4.4. Implications of Indirect WDV in Submerged Canopies

Our model shows that current-induced wave breaking occurs with various submergence ratio and vertical velocity structures (Figure 6). Additionally, it can occur at smaller  $U/c$  ratios, that is, relatively smaller opposing currents. Therefore, this process is likely to occur when waves propagate into submerged rigid mangrove forests during ebb tide. It may also occur in submerged flexible canopies, for example, saltmarshes and seagrasses, as long as the opposing current can be sufficiently diverted to the layer close to the water surface to interact with the traveling waves. The findings of the present study may be most relevant to rigid mangrove canopies. Mature mangroves are generally rigid and emergent, but newly planted/restored mangroves, for example, 1–5 years old *Kandelia Obovata* and *Rhizophora stylosa* trees, can be submerged during high tide (see Figure S5 in Supporting Information S1). Additionally, mangroves may be submerged during typhoon events by storm surges. In such cases, indirect WDV in the upper water column may also contribute to the overall wave load reduction and safety. Finally, this study confirms that the critical condition for nature-based coastal defense systems using mangroves is the case with weak following currents as it leads to minimum WDV in all the current-wave combinations (Z. Hu et al., 2014; Yin et al., 2020; Zhao et al., 2021). Thus, it should be considered as one of the critical design conditions in integrated coastal protection projects (Bouma et al., 2014; Menéndez et al., 2020).

### 5. Conclusions

To better understand indirect WDV dissipation by current-induced breaking, we conducted a set of flume experiments and analytical modeling on WDV in various hydrodynamic and canopy conditions. Although WDV with both following and opposing currents has been investigated in previous studies (Garzon et al., 2019; Z. Hu et al., 2014; Maza et al., 2015; Yin et al., 2020), the present study managed to obtain new data and insights on the WDV processes. We extended the direct  $C_D$  deriving method to waves with opposing current flows and obtained a generic  $C_D$ -Re relation covering various wave-current combinations. In this investigation, a key finding is the revealing of wave breaking triggered by opposing currents in submerged canopies. This process can be very relevant to young mangrove forests that are shallowly submerged during high tides. Although the proposed simple analytical model cannot precisely reproduce the WDV in each specific case but the general variation pattern with  $\alpha$  can be well captured. Combining a detailed experiment data set (Z. Hu et al., 2020) and the analytical model, the present study is expected to improve our understanding of the wave dissipation capacity in wetlands, especially on the indirect WDV by breaking. The obtained knowledge and model may eventually serve future nature-based coastal defense projects.

#### Acknowledgments

The authors thank three anonymous reviewers for their constructive suggestions on this study. This study was supported by the National Natural Science Foundation of China (No. 42176202) the Joint Research Project: NSFC (51761135022), NWO (ALWSD.2016.026), and EPSRC (EP/R024537/1): Sustainable Deltas, Innovation Group Project of Southern Marine Science and Engineering Guangdong Laboratory (Zhuhai; Grant no. 311021004), Guangdong Provincial Department of Science and Technology (2019ZT08G090), and Fundamental Research Funds for the Central Universities of China (20lgzd16), and 111 Project (B21018).

#### Data Availability Statement

The experiment data presented in this study can be freely accessed at <https://doi.org/10.6084/m9.figshare.13026530.v2> (Hu et al., 2020).

#### References

- Augustin, L. N., Irish, J. L., & Lynett, P. (2009). Laboratory and numerical studies of wave damping by emergent and near-emergent wetland vegetation. *Coastal Engineering*, 56(3), 332–340.
- Battjes, J. A., & Janssen, J. P. F. M. (1978). Energy loss and set-up due to breaking of random waves. *Proceedings of the 16th international conference on coastal engineering* (pp. H569–H587).
- Bouma, T. J., van Belzen, J., Balke, T., Zhu, Z., Airolidi, L., Blight, A. J., et al. (2014). Identifying knowledge gaps hampering application of intertidal habitats in coastal protection: Opportunities & steps to take. *Coastal Engineering*, 87, 147–157. <https://doi.org/10.1016/j.coastaleng.2013.11.014>
- Brevik, I., & Bjørn, A. (1979). Flume experiment on waves and currents. I. Rippled bed. *Coastal Engineering*, 3, 149–177. [https://doi.org/10.1016/0378-3839\(79\)90019-X](https://doi.org/10.1016/0378-3839(79)90019-X)

- Cao, H., Feng, W., Hu, Z., Suzuki, T., & Stive, M. J. F. (2015). Numerical modeling of vegetation-induced dissipation using an extended mild-slope equation. *Ocean Engineering*, *110*, 258–269. <https://doi.org/10.1016/j.oceaneng.2015.09.057>
- Chawla, A., & Kirby, J. T. (2002). Monochromatic and random wave breaking at blocking points. *Journal of Geophysical Research-Oceans*, *107*(C7), 3067. <https://doi.org/10.1029/2001JC001042>
- Chen, H., Ni, Y., Li, Y., Liu, F., Ou, S., Su, M., et al. (2018). Deriving vegetation drag coefficients in combined wave-current flows by calibration and direct measurement methods. *Advances in Water Resources*, *122*, 217–227. <https://doi.org/10.1016/j.advwatres.2018.10.008>
- Chen, H., & Zou, Q. (2018). Characteristics of wave breaking and blocking by spatially varying opposing currents. *Journal of Geophysical Research-Oceans*, *123*(5), 3761–3785. <https://doi.org/10.1029/2017JC013440>
- Chen, H., & Zou, Q.-P. (2019). Eulerian-Lagrangian flow-vegetation interaction model using immersed boundary method and OpenFOAM. *Advances in Water Resources*, *126*, 176–192. <https://doi.org/10.1016/j.advwatres.2019.02.006>
- Chen, M., Lou, S., Liu, S., Ma, G., Liu, H., Zhong, G., & Zhang, H. (2020). Velocity and turbulence affected by submerged rigid vegetation under waves, currents and combined wave-current flows. *Coastal Engineering*, *159*, 103727. <https://doi.org/10.1016/j.coastaleng.2020.103727>
- Currin, C. A. (2019). Chapter 30 – Living shorelines for coastal resilience. In G. M. E. Perillo, E. Wolanski, D. R. Cahoon, & C. S. Hopkins (Eds.), *Coastal wetlands* (pp. 1023–1053). Elsevier. <https://doi.org/10.1016/B978-0-444-63893-9.00030-7>
- Dalrymple, R. A., Kirby, J. T., & Hwang, P. A. (1984). Wave diffraction due to areas of energy dissipation. *Journal of Waterway, Port, Coastal, and Ocean Engineering*, *110*(1), 67–79. [https://doi.org/10.1061/\(ASCE\)0733-950X\(1984\)110:1\(67\)](https://doi.org/10.1061/(ASCE)0733-950X(1984)110:1(67))
- Dean, R., & Dalrymple, R. (1991). *Water wave mechanics for engineers and scientists* (Vol. 1–2). Tokyo: World Scientific.
- Etminan, A., Lowe, R. J., & Ghisalberti, M. (2019). Canopy resistance on oscillatory flows. *Coastal Engineering*, *152*, 103502. <https://doi.org/10.1016/j.coastaleng.2019.04.014>
- Garzon, J. L., Maza, M., Ferreira, C. M., Lara, J. L., & Losada, I. J. (2019). Wave attenuation by *Spartina* saltmarshes in the Chesapeake Bay under storm surge conditions. *Journal of Geophysical Research-Oceans*, *124*(7), 5220–5243. <https://doi.org/10.1029/2018JC014865>
- Ghisalberti, M., & Nepf, H. M. (2002). Mixing layers and coherent structures in vegetated aquatic flows. *Journal of Geophysical Research-Oceans*, *107*(C2), 33–111. <https://doi.org/10.1029/2001JC000871>
- Henry, P.-Y., Myrhaug, D., & Aberle, J. (2015). Drag forces on aquatic plants in nonlinear random waves plus current. *Estuarine, Coastal and Shelf Science*, *165*, 10–24. <https://doi.org/10.1016/j.ecss.2015.08.021>
- Horstman, E. M., Dohmen-Janssen, C. M., Narra, P. M. F., den van, B., Siemerink, M., & Hulscher, S. J. M. H. (2014). Wave attenuation in mangroves: A quantitative approach to field observations. *Coastal Engineering*, *94*, 47–62. <https://doi.org/10.1016/j.coastaleng.2014.08.005>
- Hudspeth, R. T., & Sulisz, W. (1991). Stokes drift in two-dimensional wave flumes. *Journal of Fluid Mechanics*, *230*, 209–229. <https://doi.org/10.1017/S0022112091000769>
- Hu, J., Hu, Z., & Liu, P. L.-F. (2019). Surface water waves propagating over a submerged forest. *Coastal Engineering*, *152*, 103510. <https://doi.org/10.1016/j.coastaleng.2019.103510>
- Hu, Z., Lian, S., Wei, H., Li, Y., Uijtewaal, W. S. J., & Suzuki, T. (2020). A dataset on wave propagation through vegetation with coexisting currents. *figshare*. [Dataset]. <https://doi.org/10.6084/m9.figshare.13026530.v2>
- Hu, Z., Suzuki, T., Zitman, T., Uijtewaal, W., & Stive, M. (2014). Laboratory study on wave dissipation by vegetation in combined current-wave flow. *Coastal Engineering*, *88*, 131–142. <https://doi.org/10.1016/j.coastaleng.2014.02.009>
- Huai, W., Zhang, J., Katul, G. G., Cheng, Y., Tang, X., & Wang, W. (2019). The structure of turbulent flow through submerged flexible vegetation. *Journal of Hydrodynamics*, *31*(2), 274–292. <https://doi.org/10.1007/s42241-019-0023-3>
- Infantes, E., Orfila, A., Bouma, T. J., Simarro, G., & Terrados, J. (2011). *Posidonia oceanica* and *Cymodocea nodosa* seedling tolerance to wave exposure. *Limnology & Oceanography*, *56*(6), 2223–2232. <https://doi.org/10.4319/lo.2011.56.6.2223>
- Lara, J. L., Maza, M., Ondiviela, B., Trinogga, J., Losada, I. J., Bouma, T. J., & Gordejuela, N. (2016). Large-scale 3-D experiments of wave and current interaction with real vegetation. Part 1: Guidelines for physical modeling. *Coastal Engineering*, *107*, 70–83. <https://doi.org/10.1016/j.coastaleng.2015.09.012>
- Leonardi, N., Camacina, I., Donatelli, C., Ganju, N. K., Plater, A. J., Schuerch, M., & Temmerman, S. (2018). Dynamic interactions between coastal storms and salt marshes: A review. *Geomorphology*, *301*, 92–107. <https://doi.org/10.1016/j.geomorph.2017.11.001>
- Li, C. W., & Yan, K. (2007). Numerical investigation of wave - current - vegetation interaction. *Journal of Hydraulic Engineering*, *133*(7), 7947–7803. [https://doi.org/10.1061/\(ASCE\)0733-9429](https://doi.org/10.1061/(ASCE)0733-9429)
- Liu, P. L.-F., Chang, C.-W., Mei, C. C., Lomonaco, P., Martin, F. L., & Maza, M. (2015). Periodic water waves through an aquatic forest. *Coastal Engineering*, *96*, 100–117. <https://doi.org/10.1016/j.coastaleng.2014.11.002>
- Liu, Z., Chen, Y., Zhu, D., Hui, E., & Jiang, C. (2012). Analytical model for vertical velocity profiles in flows with submerged shrub-like vegetation. *Environmental Fluid Mechanics*, *12*(4), 341–346. <https://doi.org/10.1007/s10652-012-9243-6>
- López, F., & García, M. H. (2001). Mean flow and turbulence structure of open-channel flow 895 through non-emergent vegetation @. *Journal of Hydraulic Engineering*, *127*(5), 392–402.
- Longuet-Higgins, M. S., & Stewart, R. W. (1960). Changes in the form of short gravity waves on long waves and tidal currents. *Journal of Fluid Mechanics*, *8*(4), 565–583. <https://doi.org/10.1017/S0022112060000803>
- Longuet-Higgins, M. S., & Stewart, R. W. (1961). The changes in amplitude of short gravity waves on steady non-uniform currents. *Journal of Fluid Mechanics*, *10*(4), 529–549. <https://doi.org/10.1017/S0022112061000342>
- Losada, I. J., Maza, M., & Lara, J. L. (2016). A new formulation for vegetation-induced damping under combined waves and currents. *Coastal Engineering*, *107*, 1–13. <https://doi.org/10.1016/j.coastaleng.2015.09.011>
- Lowe, R. J., Koseff, J. R., & Monismith, S. G. (2005). Oscillatory flow through submerged canopies: 1. Velocity structure. *Journal of Geophysical Research - C: Oceans*, *110*(10), 1–17.
- Mancheno, A. G., Jansen, W., Uijtewaal, W. S. J., Reniers, A. J. H. M., van Rooijen, A. A., Suzuki, T., et al. (2021). Wave transmission and drag coefficients through dense cylinder arrays: Implications for designing structures for mangrove restoration. *Ecological Engineering*, *165*, 106231. <https://doi.org/10.1016/j.ecoleng.2021.106231>
- Maza, M., Lara, J. L., Losada, I. J., Ondiviela, B., Trinogga, J., & Bouma, T. J. (2015). Large-scale 3-D experiments of wave and current interaction with real vegetation. Part 2: Experimental analysis. *Coastal Engineering*, *106*, 73–86. <https://doi.org/10.1016/j.coastaleng.2015.09.010>
- Méndez, F. J., & Losada, I. J. (2004). An empirical model to estimate the propagation of random breaking and nonbreaking waves over vegetation fields. *Coastal Engineering*, *51*(2), 103–118.
- Menéndez, P., Losada, I. J., Torres-Ortega, S., Narayan, S., & Beck, M. W. (2020). The global flood protection benefits of mangroves. *Scientific Reports*, *10*(1), 1–11. <https://doi.org/10.1038/s41598-020-61136-6>
- Möller, I., Kudella, M., Rupperecht, F., Spencer, T., Paul, M., van Wesenbeeck, B. K., et al. (2014). Wave attenuation over coastal salt marshes under storm surge conditions. *Nature Geoscience*, *7*(10), 727–731. <https://doi.org/10.1038/ngeo2251>

- Morison, J. R., Johnson, J. W., & Schaaf, S. A. (1950). The force exerted by surface waves on piles. *Journal of Petroleum Technology*, 2(5), 149–154. <https://doi.org/10.2118/950149-G>
- Nepf, H. M. (2004). Vegetated flow dynamics. In S. Fagherazzi, M. Marani, & L. K. Blum (Eds.), *Coastal and estuarine studies* (pp. 137–163). American Geophysical Union.
- Nepf, H. M. (2011). Flow over and through biota. In E. Wolanski, & D. McLusky (Eds.), *Treatise on estuarine and coastal science* (pp. 267–288). Waltham: Academic Press. Retrieved from <http://www.sciencedirect.com/science/article/pii/B9780123747112002138>
- Nepf, H. M. (2012). Flow and transport in regions with aquatic vegetation. *Annual Review of Fluid Mechanics*, 44(1), 123–142. <https://doi.org/10.1146/annurev-fluid-120710-101048>
- Nepf, H. M., & Vivoni, E. R. (2000). Flow structure in depth-limited, vegetated flow. *Journal of Geophysical Research - C: Oceans*, 105(C12), 28547–28557.
- Ondiviela, B., Losada, I. J., Lara, J. L., Maza, M., Galvan, C., Bouma, T. J., & van Belzen, J. (2014). The role of seagrasses in coastal protection in a changing climate. *Coastal Engineering*, 87, 158–168. <https://doi.org/10.1016/j.coastaleng.2013.11.005>
- Paul, M., Bouma, T. J., & Amos, C. L. (2012). Wave attenuation by submerged vegetation: Combining the effect of organism traits and tidal current. *Marine Ecology Progress Series*, 444, 31–41. <https://doi.org/10.3354/meps09489>
- Paul, M., & Gillis, L. G. (2015). Let it flow: How does an underlying current affect wave propagation over a natural seagrass meadow? *Marine Ecology Progress Series*, 523, 57–70. <https://doi.org/10.3354/meps11162>
- Pujol, D., & Nepf, H. (2012). Breaker-generated turbulence in and above a seagrass meadow. *Continental Shelf Research*, 49, 1–9. <https://doi.org/10.1016/j.csr.2012.09.004>
- Shin, J., Seo, J. Y., & Seo, I. W. (2020). Longitudinal dispersion coefficient for mixing in open channel flows with submerged vegetation. *Ecological Engineering*, 145, 105721. <https://doi.org/10.1016/j.ecoleng.2020.105721>
- Simard, M., Fatoyinbo, L., Smetanka, C., Rivera-Monroy, V. H., Castañeda-Moya, E., Thomas, N., & der Stocken, T. V. (2019). Mangrove canopy height globally related to precipitation, temperature and cyclone frequency. *Nature Geoscience*, 12(1), 40. <https://doi.org/10.1038/s41561-018-0279-1>
- Suzuki, T., Hu, Z., Kumada, K., Phan, L. K., & Zijlema, M. (2019). Non-hydrostatic modeling of drag, inertia and porous effects in wave propagation over dense vegetation fields. *Coastal Engineering*, 149, 49–64. <https://doi.org/10.1016/j.coastaleng.2019.03.011>
- Temmerman, S., Meire, P., Bouma, T. J., Herman, P. M. J., Ysebaert, T., & De Vriend, H. J. (2013). Ecosystem-based coastal defence in the face of global change. *Nature*, 504(7478), 79–83. <https://doi.org/10.1038/nature12859>
- Unna, P. J. H. (1942). Waves and tidal streams. *Nature*, 149(3773), 219–220. <https://doi.org/10.1038/149219a0>
- van Hespden, R., Hu, Z., Peng, Y., Borsje, B. W., Kleinhans, M., Ysebaert, T., & Bouma, T. J. (2021). Analysis of coastal storm damage resistance in successional mangrove species. *Limnology & Oceanography*. <https://doi.org/10.1002/lno.11875>
- van Loon-Steensma, J. M., Hu, Z., & Slim, P. A. (2016). Modelled impact of vegetation heterogeneity and salt-marsh zonation on wave damping. *Journal of Coastal Research*, 32(2), 241–252. <https://doi.org/10.2112/JCOASTRES-D-15-00095.1>
- van Loon-Steensma, J. M., Slim, P. A., Decuyper, M., & Hu, Z. (2014). Salt-marsh erosion and restoration in relation to flood protection on the Wadden Sea barrier island Terschelling. *Journal of Coastal Conservation*, 1–16. <https://doi.org/10.1007/s11852-014-0326-z>
- van Rooijen, A., Lowe, R., Ghisalberti, M., Conde-Frias, M., & Tan, L. (2018). Predicting current-induced drag in emergent and submerged aquatic vegetation canopies. *Frontiers in Marine Science*, 5. Retrieved from <https://www.frontiersin.org/article/10.3389/fmars.2018.00449>
- van Veelen, T. J., Karunarathna, H., & Reeve, D. E. (2021). Modelling wave attenuation by quasi-flexible coastal vegetation. *Coastal Engineering*, 164, 103820. <https://doi.org/10.1016/j.coastaleng.2020.103820>
- Vuik, V., Jonkman, S. N., Borsje, B. W., & Suzuki, T. (2016). Nature-based flood protection: The efficiency of vegetated foreshores for reducing wave loads on coastal dikes. *Coastal Engineering*, 116, 42–56. <https://doi.org/10.1016/j.coastaleng.2016.06.001>
- Vuik, V., van Vuren, S., Borsje, B. W., van Wesenbeeck, B. K., & Jonkman, S. N. (2018). Assessing safety of nature-based flood defenses: Dealing with extremes and uncertainties. *Coastal Engineering*, 139, 47–64. <https://doi.org/10.1016/j.coastaleng.2018.05.002>
- Wang, B., Guo, X., & Mei, C. C. (2015). Surface water waves over a shallow canopy. *Journal of Fluid Mechanics*, 768, 572–599. <https://doi.org/10.1017/jfm.2015.110>
- Yang, S. L., Shi, B. W., Bouma, T. J., Ysebaert, T., & Luo, X. X. (2012). Wave attenuation at a salt marsh margin: A case study of an exposed coast on the Yangtze estuary. *Estuaries and Coasts*, 35(1), 169–182.
- Yao, P., Chen, H., Huang, B., Tan, C., Hu, Z., Ren, L., & Yang, Q. (2018). Applying a new force-velocity synchronizing algorithm to derive drag coefficients of rigid vegetation in oscillatory flows. *Water*, 10(7), 906. <https://doi.org/10.3390/w10070906>
- Yin, Z., Wang, Y., Liu, Y., & Zou, W. (2020). Wave attenuation by rigid emergent vegetation under combined wave and current flows. *Ocean Engineering*, 213, 107632. <https://doi.org/10.1016/j.oceaneng.2020.107632>
- Ysebaert, T., Yang, S.-L., Zhang, L., He, Q., Bouma, T. J., & Herman, P. M. J. (2011). Wave attenuation by two contrasting ecosystem engineering salt marsh macrophytes in the intertidal pioneer zone. *Wetlands*, 31(6), 1043–1054. <https://doi.org/10.1007/s13157-011-0240-1>
- Yu, Y.-Y. (1952). Breaking of waves by an opposing current. *Eos, Transactions American Geophysical Union*, 33(1), 39–41. <https://doi.org/10.1029/TR033i001p00039>
- Zhao, C., Tang, J., Shen, Y., & Wang, Y. (2021). Study on wave attenuation in following and opposing currents due to rigid vegetation. *Ocean Engineering*, 236, 109574. <https://doi.org/10.1016/j.oceaneng.2021.109574>
- Zheng, J., Mase, H., Demirebilek, Z., & Lin, L. (2008). Implementation and evaluation of alternative wave breaking formulas in a coastal spectral wave model. *Ocean Engineering*, 35(11–12), 1090–1101.